GUFBD / *GUJS* (2022) IOCENS'21 Ek Sayısı: 89-97
DOI: 10.17714/gumusfenbil.1030049 Araştırma Makalesi / *Research Article*

Investigation of the X-ray fluorescence parameters and valance electronic structure for Ni in Ni-B/hBN coating materials with doped TMAB and saccharine

Ni-B/hBN katkılı TMAB ve sakarinli kaplama malzemelerinde Ni için X-ışını floresans parametrelerinin ve valans elektronik yapısının incelenmesi

Oguz Kagan KOKSAL[*1,2a] **Ismail Hakki KARAHAN**[3b]
[1]*Adıyaman University, Faculty of Engineering, Department of Electrical-Electronics Engineering, 02040, Adıyaman*
[2]*Karadeniz Technical University, Faculty of Science, Department of Physics, 61080, Trabzon*
[3]*Hatay Mustafa Kemal University, Faculty of Science Literature, Department of Physics, 31070, Hatay*

• Geliş tarihi / *Received*: 29.11.2021 • Düzeltilerek geliş tarihi / *Received in revised form*: 20.04.2022 • Kabul tarihi / *Accepted*: 19.09.2022

Abstract
In this investigation, K shell valance electronic structure of Ni in Ni-B alloy coatings were studied by means of collecting the X-ray emission and XRD spectra. The data obtained were evaluated in terms of the K beta/K alpha X-ray intensity ratios and XRD data. The coated alloys were fabricated with using different concentrations of hexagonal boron nitride (hBN) for this study by electrochemical storage method. Besides saccharine and trimethylamine borane complex (TMAB) were added the current samples at constant concentration. The current specimens were excited by 59.5 keV photons from a 241Am annular radioactive source. K shell X-rays emitted by the specimens were detected by means of an Ultra-LEGe detector with a resolution of 150 eV at 5.9 keV. The K shell X-ray intensity ratios of Ni-B alloys are checked with pure Ni. Variations in the current outcomes were interpreted by the variation in valence electronic structures of Ni in Ni-B/hBN coating materials with doped TMAB and saccharine.

Keywords: Intensity ratio, K shell, XRD, XRF, Valance electronic structure

Öz
Bu araştırmada, Ni-B alaşımlı kaplamalarda Ni'nin K kabuğu değerlik elektronik yapısı, X-ışını emisyonu ve XRD spektrumları toplanarak incelenmiştir. Elde edilen veriler K beta/K alfa X-ışını yoğunluk oranları ve XRD verileri açısından değerlendirildi. Kaplanmış alaşımlar, bu çalışma için farklı konsantrasyonlarda altıgen bor nitrür (hBN) kullanılarak elektrokimyasal depolama yöntemiyle üretilmiştir. Mevcut örneklere sabit konsantrasyonda sakarin ve trimetilamin boran kompleksi (TMAB) ilave edildi. Mevcut örnekler, 241 Am halka şeklindeki radyoaktif kaynaktan gelen 59.5 keV fotonları tarafından uyarıldı. Örneklerden yayılan K kabuk X-ışınları, 5,9 keV'de 150 eV çözünürlüğe sahip bir Ultra-LEGe dedektörü vasıtasıyla tespit edildi. Ni-B alaşımlarının K kabuğu X-ışını yoğunluk oranları saf Ni ile kontrol edildi. Mevcut sonuçlardaki değişimler, katkılı TMAB ve sakarin içeren Ni-B/hBN kaplama malzemelerinde Ni'nin değerlik elektronik yapılarındaki değişim ile yorumlanmıştır.

***Keywords**: Şiddet oranı, K kabuğu, XRD, XRF, Değerlik elektron yapısı*

[*a] Oguz Kagan KOKSAL; okoksal@ktu.edu.tr, Phone: 90 416 223 38 00 orcid.org/0000-0003-2671-6683
[b] orcid.org/0000-0002-8297-3521

1. Introduction

1. Giriş

The XRF technique is a non-destructive spectroscopic technique that provides interaction between material and X-ray photons with a small amount of sample. In this sense, Energy dispersive X-ray fluorescence (EDXRF) method is one of the most widely used techniques and the K-shell X-ray intensity ratios, which vary according to the chemical and physical facilities of the samples, present the knowledge regarding the valence electron structure of the 3d metals (Pawłowski et al., 2002). X-ray spectra provide us the important information on issues such as the vacancy transfer probabilities, production cross sections, estimation of the effects of the valence electron structure and chemical environment on the intensity ratio, as well as the element contents (Gójska et al., 2020). Therefore, the K shell X-ray intensity ratios of 3d metals have been investigated by many of investigators (Alım et al., 2016; Garmay et al., 2017; Gójska et al., 2020; Perişanoğlu & Demir, 2015; Perişanoğlu et al., 2020; Uğurlu et al., 2019; Uğurlu et al, 2017).

Transition metals have special uses mainly due to their hardness, high density, good thermal conductivity, high melting and boiling temperatures. Although some are lack of this feature, some have a very important place in our lives, like nickel (Uğurlu & Demir, 2020). Ni-B coatings; It is widely utilized in areas such as automotive, aerospace, petro chemistry, textile and electronics due to its high hardness, resistance to corrosion and strong resistance to abrasion. However, it is still being tried to improve its properties with various studies in order to be used in these areas (Chang et al., 2017; Matsui et al 2017; Matsui et al, 2018; Mirak & Akbari, 2018; Ogihara et al., 2012; Onoda et al., 1999; Sanyal et al., 2013; Shakoor et al., 2014a, 2014b; Tozar, 2020; Ünal & Karahan, 2018a, 2018b; Waware et al., 2018).

Although it has been revealed that saccharine does not have a positive effect on properties such as corrosion, abrasion and hardness, it has been revealed that the TMAB has an effect on the particle size. In addition, it has been shown that saccharine substance reduces the concentration value of the metal in the alloy (Bahramian, et al., 2018; Ignatova & Marcheva, 2016; Sanyal et al., 2013; Sanyal & Jagirdar, 2012).

When looking at previous studies, it seems that the element Ni is coated with hBN by means of adding TMAB and saccharin at a constant rate (Ikram et al., 2020; Siegel et al., 2019; Smid et al., 2012; Tyagi et al., 2010; Yıldırım et al., 2019; Zhang et al., 2010). It has been revealed that TMAB adheres to the surface of Ni/B composite coatings and creates micro-caves on the surface due to electric charges (Sheu et al., 2021).

In this study, different concentrations of hBN coating material were added to the Ni-B alloy. TMAB and saccharine were also added at a constant concentration. The main goal of the current investigation is to interpret the valence electronic arrangement of Ni in Ni-B/hBN whether TMAB and saccharine substances added to improve some properties of the current alloys affect the valance electron structure with using the K shell intensity ratios.

2. Material and methods

2. Malzeme ve yöntem

2.1. Sampling

2.1. Numune

Ni-B/hBN alloy coatings were electrodeposited on St-37 low carbon mild steel substrate in Watts type nickel electrolyte and the bath contains nickel sulphate ($NiSO_4.6H_2O$) (240 g/l) , boric acid (H_3BO_3) (30 g/l) and nickel chloride ($NiCl_2.6H_2O$) (45 g/l) as source of nickel, trimethylamine borane complex (TMAB) (5 g/l) gas source of boron, hBN (5,10,15 and 20 g/l) as reinforcing particles, saccharine as grain refining agent, sodium dodecyl sulphate (SDS) (0.5 g/l) as surfactant and saccharine at 2 g/l. Table 1 shows that production and bath facilities. The other parameters such as ultrasonic stirring, temperature, pH, preparing time, stirring speed and current density were adjusted as ; 30 minutes, 43°C, 4, 60 minutes, 500-600 rpm and 50 mA/cm^2; respectively. The pure nickel and nickel-bor hBN coating composite material alloys used in this work are manufactured by (Ünal & Karahan, 2018b) and are tabulated in the Table 1 with their production facility. The concentration values in Table 1 are weight percentage values and the EDX result was obtained for these concentration values.

Table 1. Sample production process and concentration values
Tablo 1. *Numune üretme süreci ve konsantrasyon değerleri*

Production Facilities	Pure Ni	A22	A24	A25
Ni %	100	85.74	84.7	87.2
B %	-	13.2	14.10	11.15
N %	-	1.05	1.19	1.58
H_3BO_3 (g/l)	-		30	
$NiSO_4$ (g/l)	-		240	
$NiCl_2$ (g/l)	-		45	
TMAB (g/l)	-		3	
Saccharine (g/l)	-		2	
hBN (g/l)	-	5	15	20
SDS (g/l)	-		0.5	
Ultrasonic stirring (min.)	-		30	
Temparatute (^{0}C)	-		43±1	
pH	-		4	
The duration of deposition (minute)	-		60	
The ratio of agitation(rpm)	-		500-600	
Current Density (mA/cm^2)	-		50	

2.2. EDXRF measurements
2.2. EDXRF ölçümleri

The experiment geometry consists of an Ultra Low Energy Germanium detector which has thickness of 5mm and energy resolution 150 eV at 5.96 keV, radioactive source which emits 59.5 keV photons from 50 mCi ^{241}Am and the target are illustrated which is covered by a lead collimator in figure 1.

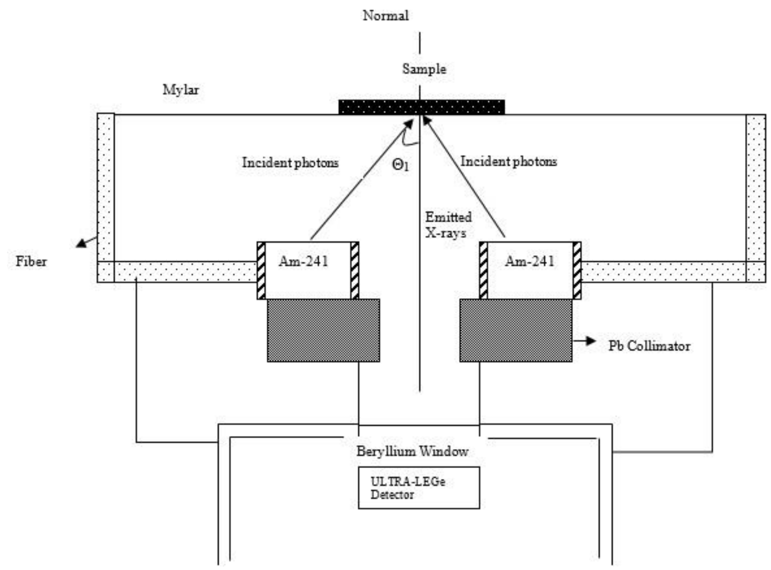

Figure 1. The current experimental geometry with 50 mCi ^{241}Am source with the angles
Şekil 1*. 50 mCi ^{241}Am kaynaklı kullanılan deney geometrisi*

The experimental set up was established so that the angle of emitted primary photon flux with the specimen surface was 45° and the X-ray fluorescence beam from the specimen was 90° with the specimen surface. In this experiment, the counting time was set to 10000 s for each sample. In the current investigation, the spectra analysis was made with using WinAxil Mitac 4.0 version program for the designation of the peak analysis. First of all required points subtracting as marking were removed thus background subtraction is done and X ray peaks are fitted as Gaussian functions with using PFM (Peak Fitting Module) in this program.

2.3. XRD measurements
2.3. XRD ölçümleri

The X-ray diffraction pattern of Ni-B/hBN composite material was obtained with using Rigaku X-ray diffractometer performed for 40 kV potential and 30 mA current with Cu K_α photon.

2.4. Calculations

2.4. Hesaplamalar

(K_β/K_α) intensity ratio was calculated with the equation shown below:

$$\frac{I_{K\beta}}{I_{K\alpha}} = \frac{N_{K\beta}\beta_{K\alpha}\varepsilon_{K\alpha}}{N_{K\alpha}\beta_{K\beta}\varepsilon_{K\beta}} \quad (1)$$

where $N_{(K\alpha)}$ and $N_{(K\beta)}$ are the net photon numbers under the K_α and K_β peaks, $\varepsilon(K_\alpha)$ and $\varepsilon(K_\beta)$ are the detector efficiencies of K_α and K_β, $\beta_{(K\alpha)}$ and $\beta_{(K\beta)}$ are the self-absorption correction factors determined as following equation:

$$\beta = \frac{1 - \exp\left[-\left(\frac{\mu_{inc}}{\cos\theta_1} + \frac{\mu_{emt}}{\cos\theta_2}\right)t\right]}{\left(\frac{\mu_{inc}}{\cos\theta_1} + \frac{\mu_{emt}}{\cos\theta_2}\right)t} \quad (2)$$

where μ_{inc} and μ_{emt} are the mass attenuation coefficients (cm^2/g) of incident photons and emitted K X-rays respectively. $\theta_1$and θ_2 are the angles of incident photons and emitted X-rays with respect to the normal at the surface of the specimen in the current experimental geometry and t is the mass thickness of the specimen in g/cm^2.

$I_0G\varepsilon$ term which is consist of the primary photon beam, geometrical factor and the efficiency of the radiation detector, were gathered the K_α and K_β X-ray spectra K, Ca, Ti, Cr, Mn, Co, Ni, Zn, Ga, As, Se, Br, Y, Mo, Sn and Te in the same experimental set-up utilizing the following formula:

$$I_0G\varepsilon_{Ki} = \frac{N_{Ki}}{\sigma_{Ki}\beta_{Ki}m}[i = \alpha, \beta] \quad (3)$$

Where the terms N_{Kx} and β_{Kx} are the net photon numbers under the K_x peak and $\beta_{(Ki)}$ is the self-absorption correction factors, respectively. m_i is the chemical composition (g/cm^2). σ_{Kx} X-ray production cross-section was determined with the help of the formula below:

$$\sigma_{Kx} = \sigma_K(E)\omega_K F_{Kx}\ (x = \alpha \text{ and } \beta) \quad (4)$$

Where σ_K (E) is the K-shell photoionization cross-section of the current element for the excitation energy E, ω_K is the K-shell fluorescence yield, and F_{Kx} is the emission rate of the fractional X-ray for K_α and K_β X-rays. The factor $I_0G_\varepsilon K_x$ was plotted and fitted as a function of energy utilizing the polynomials:

$$I_0G\varepsilon_{Kx} = A_0 + A_1E_i + A_2E_i^2 + A_3E_i^3 (\text{1st part}) \quad (5)$$

$$I_0G\varepsilon_{Kx} = B_0 + B_1E_i + A_2E_i^2\ (\text{2nd part}) \quad (6)$$

where E_i is the K_α or K_β X-ray energy. The deviation $I_0G\varepsilon Kx$ as a function of the K X-ray energy is illustrated in Figure 2. The formulas (5) and (6) correspond to the first and second parts of Figure 2, respectively.

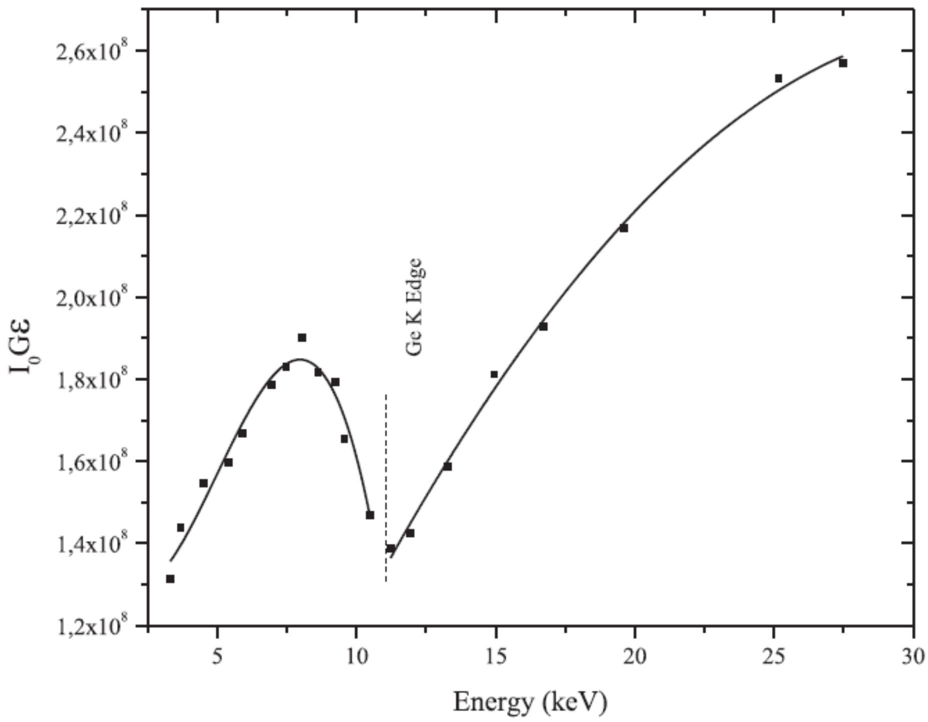

Figure 2 . The variation of the factor $I_0G\varepsilon$ as a function of the mean K X-ray energy for 50 mCi ^{241}Am source

Şekil 2. *50 mCi ^{241}Am için ortalama K X-Işını enerjisinin fonksiyonu olarak dedektör verim eğrisi*

3. Results and discussions

3. Sonuçlar ve tartışma

The chemical environments of the elements that make up the alloy affect the chemical bond states, crystal structures, and characteristic X-ray emission and absorption probabilities in general. The K X-ray spectrum of Ni for specimen A25 is illustrated in the figure 3. The horizontal axis represents the energy (keV) and the vertical axis represents the photon counts. The horizontal axis shows the angle and the vertical axis shows the intensity. When looking at the X-ray spectrum of the A 25 sample in the figure 3, it is seen that there is no shift in the energies corresponding to the peaks of the Ni K alpha and beta peaks. This demonstrates the reliability of the XRF system.

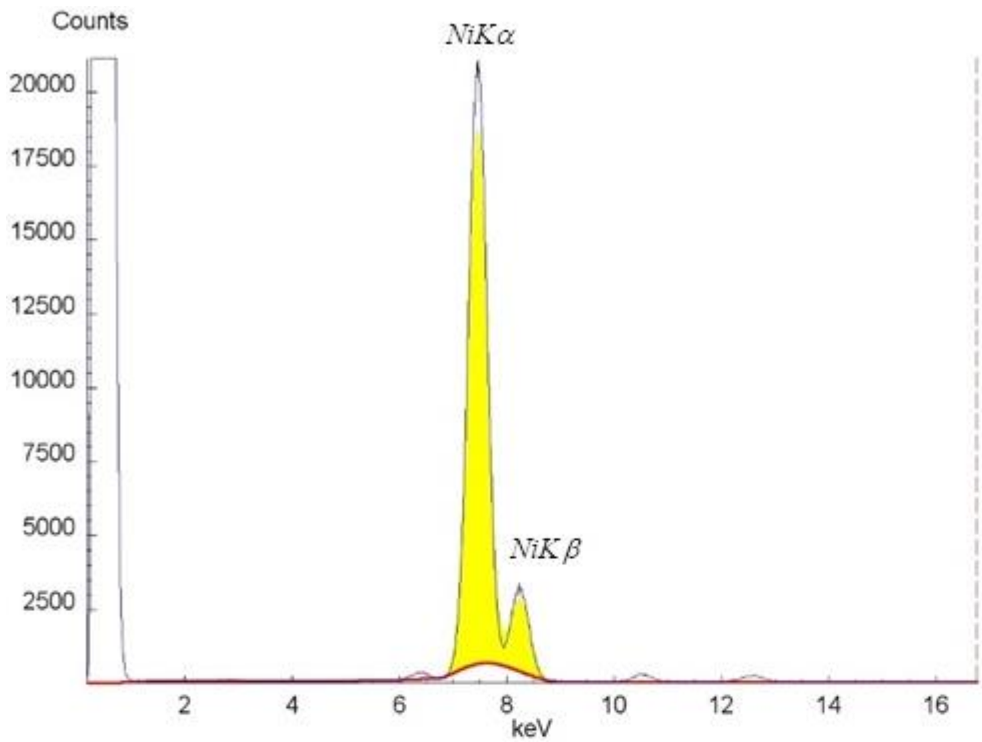

Figure 3. K X-ray spectra of Nickel measured with 50 mCi ^{241}Am
Şekil 3. *Nikel elementine ait ölçülen K X-ışını spektrumu*

The XRD spectra was shown as Figure 4. The added hBN, TMAB and saccharin substances while forming the alloy affected the 3d electron populations and as a result, the K shell X-ray intensity ratios is changed. Looking at the XRD peaks in the figure 4, it is seen that the Ni peaks change with the addition of hBN. Ni(111), Ni(200), Ni(220) and Ni(311) peak intensities in the XRD spectrum decrease as hBN is added. In the previous studies, it has been reported that the concentration values change with the addition of saccharin and the particle size changes with the addition of TMAB. Such conditions affect the electron density and can change the K shell X-ray intensity ratios (Bahramian et al., 2018; Cengiz, Köksal, Apaydın, Karahan, & Ünal, 2019; Ignatova & Marcheva, 2016).

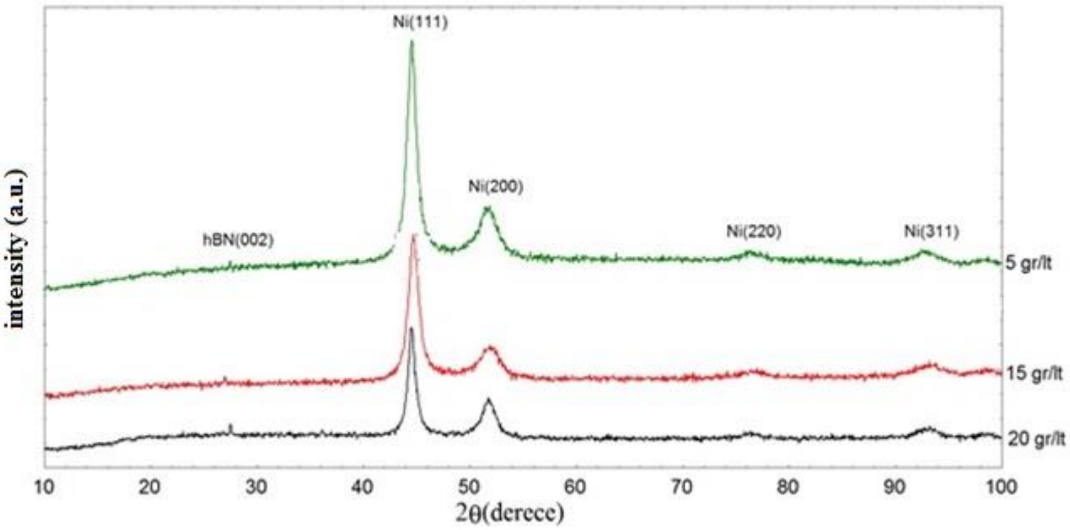

Figure 4. XRD Spectra
Şekil 4. *XRD spektrumları*

The SEM images were illustrated in the Figure 5 for the current samples.

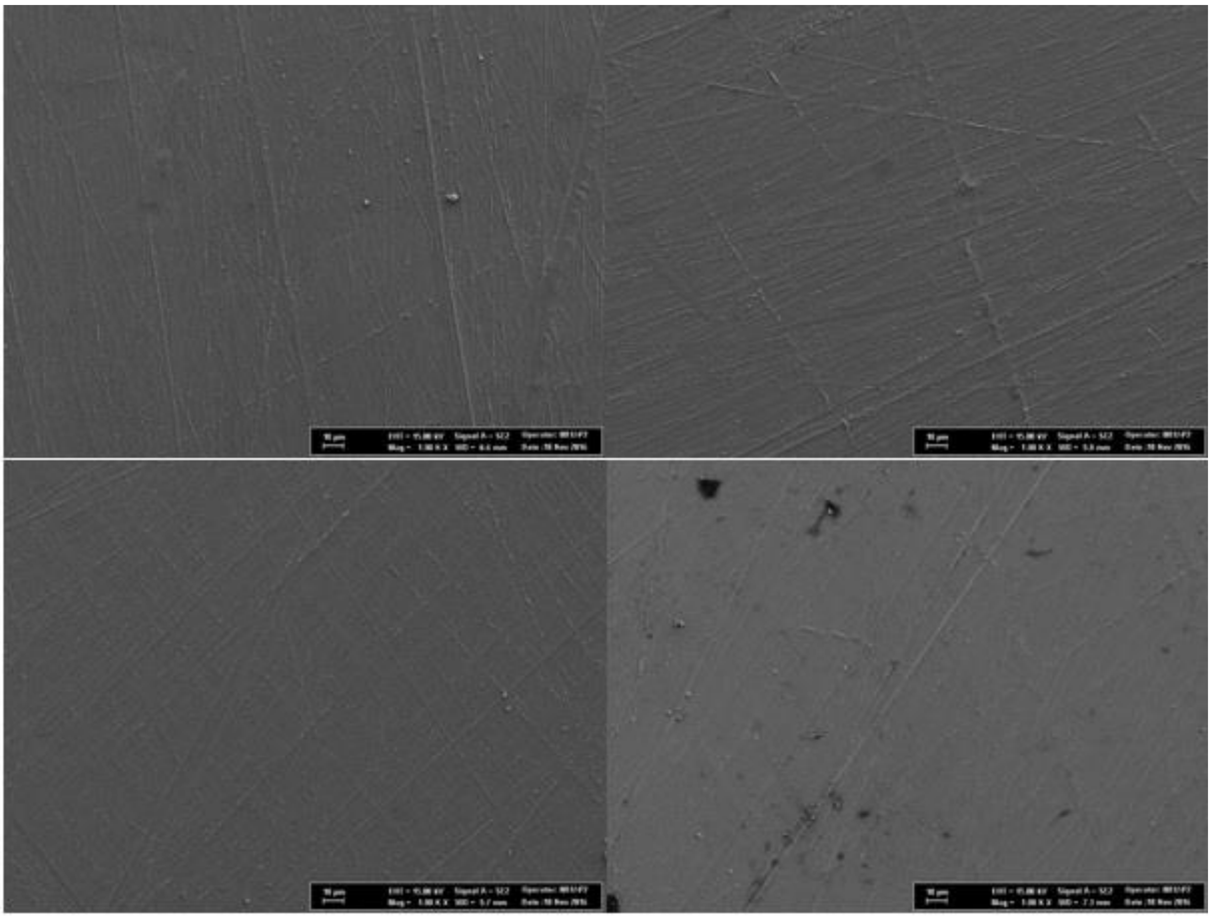

Figure 5. SEM Images (A7, A22, A24 and A25; respectively)
Şekil 5*. SEM görüntüleri (sırasıyla, A7, A22, A24 and A25)*

In this study, the experimental results are given for the $I_{K\beta}/I_{K\alpha}$ of Ni, B and N composite materials with doped TMAB and saccharin. When looking at the table 2, the intensity ratio for pure Ni is tabulated Scofield, Coulomb and Babushin values. The current values are consistent with Scofield's theoretical value.

Table 2. Experimental K X-Ray Intensity Ratios of Ni in NiB alloy coatings ($I_{K\beta}/I_{K\alpha}$); Relative K X-Ray Intensity Ratios of Ni in NiB alloy coatings ($R_{K\beta}/R_{K\alpha}$) with respect to Pure Ni.
Tablo 2. *Saf Ni elementine göre NiB alaşımının içindeki Ni için deneysel K X-ışını şiddet oranı ($I_{K\beta}/I_{K\alpha}$); NiB alaşımının içindeki Ni için göreli K X-ışını şiddet oranları ($R_{K\beta}/R_{K\alpha}$)*

Specimen	**Exp.** $I_{K\beta}/I_{K\alpha}$	$R_{K\beta}/R_{K\alpha}$	**Theo.** Scofield 1974 (Scofield, 1974)		Coulomb gauge (Polasik, 1998)	Babushin gauge
				$3d^8 4s^2$	0.1361	0.1374
Pure Ni	0.1236±0.0074	1.0000	0.1227	$3d^9 4s^1$	0.1333	0.1346
				$3d^{10}$	0.1313	0.1325
A22	0.1358±0.0081	1.3182±0.0079	---		---	---
A24	0.1413±0.0085	1.3717±0.0082	---		---	---
A25	0.1408±0.0084	1.3670±0.0082	---		---	---

However, when compared with the Coulomb and Babuskin gauges for all cases, it is seen that the K shell X-Ray intensity ratio is smaller for pure Nickel than Scofield theoretical value. It is seen that the K shell X-ray intensity ratios of the alloys are larger than pure Nickel and when considering the Babuskin and coulomb gauges. The alloying effect on the intensity ratio can be changed by the change of valence electron structure due to the altered shielding by the repositioning of the charges in the d orbital. This change is related to the rearrangement of electrons between 3d (4s, 4p). If the electron in the d orbital of one element is transferred to the d orbital of the other element, it is changed for different alloy compositions. Therefore, the intensity ratio depends on the alloy compositions. With the addition of saccharine, this composition changed and the intensity ratios changed compared to the saccharine-free Ni-B alloys (Brunner, Nagel, Hartmann, & Arndt, 1982). The changes in the K-shell X-ray intensity ratios are thought to be due to the alloying effect. This significant difference is caused by the charge transfer and rearrangement processes. So the valence electron structure can be affected by this situation.

The overall error in the Table 3 is predicted as 6%. This error is the quadrature sum of the errors in the various parameters utilized to consider the K-shell fluorescence parameters, i.e. counting statistics (2%) ($N(K_i)$ ($i=\alpha, \beta$)), different parameters used to evaluate factor (2%) ($I_0 G \varepsilon K_x$), Absorption coefficients correction at incident and emitted photon energies (1.5%) (β) and Weight and thickness of the samples (1%) (t).

Table 3. Uncertainties in the quantities used to determine the parameters
Tablo 3. Deneysel paramaterelerin belirlenmesindeki hatalar

Quality	**Reason for Error**	**Uncertainty (%)**
$N(K_i)$ ($i=\alpha, \beta$)	Counting statistic	≤ 2
$I_0 G \varepsilon_{K_i}$	Different parameters used to evaluate factor	≤ 2
β	Absorption coefficients correction at incident and emitted photon energies	≤ 1.5
t	Weight and thickness of the samples	≤ 1

4. Conclusion
4. Tartışma

In this investigation, the K-shell X-ray intensity ratios of nickel in pure Ni and TMAB and saccharine doped Ni-B alloy coatings were experimentally calculated. While the experimental K-shell X-ray intensity ratios of pure nickel are consistent with the theoretical values of Scofield, they are lower than the values of Coulomb and Babuskin gauges. In previous studies, it has been stated that saccharin affects the element concentration values, while TMAB changes the grain size. It is seen that these changes can change the intensity ratios. In addition, it has been revealed that TMAB adheres to the surface of Ni/B composite coatings and creates micro-caves on the surface due to electric charges. Another reason for the decrease in the intensity ratio in the alloys used is the possibility of enhancement boron and nitrogen by the characteristic K_α and K_β peaks of Nickel. It is thought that this situation will affect the valence electron structure. Therefore, this phenomenon, charge transfer and rearrangement processes also affect the valence electron structure of pure nickel.

Author contribution
Yazar katkısı

O.K. Koksal: Writing – original draft, Visualization, Validation, Supervision, Software, Resources, Project administration, Methodology, Investigation, Formal analysis, Data curation, Conceptualization; I.H. Karahan: Writing – review & editing, Supervision.

Declaration of ethical code
Etik beyanı

The authors of this article declare that the materials and methods used in this study do not require ethical committee approval and/or legal-specific permission.

Conflicts of interest
Çıkar çatışması beyanı

The authors declare that they have no known competing financial interests or personal relationships that could have appeared to influence the work reported in this paper.

References
Kaynaklar

Alım, B., Han, İ., & Demir, L. (2016). Effect of external magnetic field on valence-electron structures of Fe and Ni in Invar, Permalloy and the other Fe–Ni alloys by using Kβ-to-Kα X-ray intensity ratios. Applied Radiation and Isotopes, 112, 5-12.

Bahramian, A., Eyraud, M., Vacandio, F., & Knauth, P. (2018). Improving the corrosion properties of amorphous Ni-P thin films using different additives. Surface and Coatings Technology, 345, 40-52.

Brunner, G., Nagel, M., Hartmann, E., & Arndt, E. (1982). Chemical sensitivity of the Kβ/Kα X-ray intensity ratio for 3d elements. Journal of Physics B: Atomic and Molecular Physics, 15(24), 4517.

Cengiz, E., Köksal, O. K., Apaydın, G., Karahan, İ. H., & Ünal, E. (2019). Determination of valence electronic structure of Ni in Ni-B alloy coatings using Kβ-to-Kα X-ray intensity ratios. Applied Radiation and Isotopes, 144, 24-28.

Chang, C.-R., Hou, K.-H., Ger, M.-D., & Wang, J.-R. (2017). Characteristics of nickel boron coatings prepared by direct current electrodeposition technique. Int. J. Electrochem. Sci., 12, 2055-2069.

Garmay, A., Oskolok, K., & Monogarova, O. (2017). The use of the ratios of intensities of spectral lines for X-ray fluorescence analysis of metal alloys and oxide materials. Moscow University Chemistry Bulletin, 72(1), 49-55.

Gójska, A. M., Kozioł, K., Mišta-Jakubowska, E. A., & Diduszko, R. (2020). Determination of the Kβ/Kα intensity ratios of silver in Ag-Cu alloys. Nuclear Instruments and Methods in Physics Research Section B: Beam Interactions with Materials and Atoms, 468, 65-70.

Ignatova, K. N., & Marcheva, Y. S. (2016). Effect of saccharine on the properties of Ni-Co alloy coatings deposited in citrate electrolytes. Paper presented at the 2016 XXV International Scientific Conference Electronics (ET).

Ikram, M., Hassan, J., Imran, M., Haider, J., Ul-Hamid, A., Shahzadi, I., . . . Ali, S. (2020). 2D chemically exfoliated hexagonal boron nitride (hBN) nanosheets doped with Ni: synthesis, properties and catalytic application for the treatment of industrial wastewater. Applied Nanoscience, 10, 3525-3528.

Matsui, I., Li, M., & Omura, N. (2017). Fabricating Bulk Nanocrystalline Ni–W–B Alloys by Electrodeposition. Materials Transactions, 58(7), 1038-1041.

Matsui, I., Omura, N., Yamamoto, T., & Takigawa, Y. (2018). Electrodeposition with intermittent addition of trimethylamine borane to produce ductile bulk nanocrystalline Ni–B alloys. Surface and Coatings Technology, 337, 411-417.

Mirak, M., & Akbari, A. (2018). Microstructural characterization of electrodeposited and heat-treated Ni-B coatings. Surface and Coatings Technology, 349, 442-451.

Ogihara, H., Udagawa, K., & Saji, T. (2012). Effect of boron content and crystalline structure on hardness in electrodeposited Ni–B alloy films. Surface and Coatings Technology, 206(11-12), 2933-2940.

Onoda, M., Shimizu, K., Tateishi, Y., & Watanabe, T. (1999). Mechanism of boron codeposition in electrodeposited Ni-B alloy films and calculation of the amount of codeposited boron. Transactions of the IMF, 77(1), 44-48.

Pawłowski, F., Polasik, M., Raj, S., Padhi, H., & Basa, D. (2002). Valence electronic structure of Ti, Cr, Fe and Co in some alloys from Kβ-to-Kα X-ray intensity ratio studies. Nuclear Instruments and Methods in Physics Research Section B: Beam Interactions with Materials and Atoms, 195(3-4), 367-373.

Perişanoğlu, U., & Demir, L. (2015). A study of K shell X-ray intensity ratios of NixCr1− x alloys in external magnetic field and determination of effective atomic numbers of these alloys. Radiation Physics and Chemistry, 110, 119-125.

Perişanoğlu, U., Kavaz, E., Urtekin, E., & Demir, L. (2020). Examining alloying effect on KX ray intensity ratios and chemical shifts of the Zn, Mn and mixed spinel ferrites. Applied Radiation and Isotopes, 156, 108980.

Polasik, M. (1998). Influence of changes in the valence electronic configuration on the K beta-to-K alpha x-ray intensity ratios of the 3d transition metals. Physical Review A, 58(3), 1840-1845.

Sanyal, U., Davis, D. T., & Jagirdar, B. R. (2013). Bimetallic core–shell nanocomposites using weak reducing agent and their transformation to alloy nanostructures. Dalton Transactions, 42(19), 7147-7157.

Sanyal, U., & Jagirdar, B. R. (2012). Metal and alloy nanoparticles by amine-borane reduction of metal salts by solid-phase synthesis: atom economy and green process. Inorganic Chemistry, 51(23), 13023-13033.

Scofield, J. H. (1974). Relativistic Hartree-Slater values for K and L X-ray emission rates. Atomic Data and Nuclear Data Tables, 14, 121-137.

Shakoor, R., Kahraman, R., Waware, U. S., Wang, Y., & Gao, W. (2014a). Synthesis and properties of electrodeposited Ni-B-Zn ternary alloy coatings. Int. J. Electrochem. Sci, 9, 5520.

Shakoor, R., Kahraman, R., Waware, U. S., Wang, Y., & Gao, W. (2014b). Synthesis and properties of electrodeposited Ni–B–CeO2 composite coatings. Materials & Design, 59, 421-429.

Sheu, H.-H., Wang, Q.-Y., Huang, P.-C., Cheng, A.-Y., Liu, Y.-M., Hou, K.-H., & Ger, M.-D. (2021). Effect of Trimethylamine Borane (TMAB) on the Corrosion Resistance and Mechanical Properties of Nickel-Based Composite Coatings. International Journal of Electrochemical Science, 16(4).

Siegel, G., Gryzbowcki, G., Hilton, A., Muratore, C., & Snure, M. (2019). Growth of Multi-Layer hBN on Ni (111) Substrates via MOCVD. Crystals, 9(7), 339.

Smid, I., Segall, A., Walia, P., Aggarwal, G., Eden, T., & Potter, J. (2012). Cold-sprayed Ni-hBN self-lubricating coatings. Tribology transactions, 55(5), 599-605.

Tozar, A. (2020). Investigating the hexadecylamine as a new nonionic surfactant candidate for electrodeposition of wear-resistant metal-matrix composites. Surface engineering, 36(9), 990-999.

Tyagi, R., Xiong, D. S., Li, J., & Dai, J. (2010). Elevated temperature tribological behavior of Ni based composites containing nano-silver and hBN. Wear, 269(11-12), 884-890.

Uğurlu, M., Alım, B., & Demir, L. (2019). The relationship between the external magnetic field and K X-ray intensity ratios of immiscible MoxAg1-x alloys. Radiation Physics and Chemistry, 165, 108396.

Uğurlu, M., Alım, B., Han, I., & Demir, L. (2017). Delocalization and charge transfer studies of PERMENDUR49, KOVAR and Ti50Co50 alloys from relative K X-ray intensity ratios. Journal of Alloys and Compounds, 695, 2619-2627.

Uğurlu, M., & Demir, L. (2020). Relative K X-ray intensity ratios of the first and second transition elements in the magnetic field. Journal of Molecular Structure, 1203, 127458.

Ünal, E., & Karahan, I. (2018a). Effects of ultrasonic agitation prior to deposition and additives in the bath on electrodeposited Ni-B/hBN composite coatings. Journal of Alloys and Compounds, 763, 329-341.

Ünal, E., & Karahan, I. (2018b). Production and characterization of electrodeposited Ni-B/hBN composite coatings. Surface and Coatings Technology, 333, 125-137.

Waware, U. S., Hamouda, A., & Wasekar, N. P. (2018). Mechanical properties, thermal stability and corrosion behavior of electrodeposited Ni-B/AlN nanocomposite coating. Surface and Coatings Technology, 337, 335-341.

Yıldırım, Ç. V., Sarıkaya, M., Kıvak, T., & Şirin, Ş. (2019). The effect of addition of hBN nanoparticles to nanofluid-MQL on tool wear patterns, tool life, roughness and temperature in turning of Ni-based Inconel 625. Tribology International, 134, 443-456.

Zhang, J., Tu, R., & Goto, T. (2010). Preparation of Ni-precipitated hBN powder by rotary chemical vapor deposition and its consolidation by spark plasma sintering. Journal of Alloys and Compounds, 502(2), 371-375.